ORIGINAL PAPER

A systematic study on the fabrication of transparent nanopaper based on controlled cellulose nanostructure from oil palm empty fruit bunch

Athanasia Amanda Septevani[1,2] · Dian Burhani[3] · Yulianti Sampora[4] · Indriyati[5] · Shobih[6] · Erlyta Septa Rosa[6] · Dewi Sondari[3] · Nur Ita Margyaningsih[7] · Melati Septiyani[4] · Fitra Yurid[1] · Aniek Sri Handayani[2]

Abstract

Cellulose nanopaper (CNP) is a new potential candidate for flexible biopolymer substrate made of nanocellulose (NC). We systematically studied the effect of NC production from oil palm empty fruit bunch using the different types of acid hydrolysis based on sulphuric acid (NCs) as well as phosphoric acid (NCp) at varied temperatures regarding their morphology and crystallinity on the final properties of CNP. Both CNP from NCs (CNPs) and NCp (CNPp) exhibited higher optical transparency than conventional micropaper. In terms of mechanical properties, CNPs possessed an exceptional improvement of up to 200% compared to micropaper. CNPp specifically produced higher mechanical properties compared to CNPs. The stronger tensile strength of CNPp was attributed to a higher aspect ratio and thus a more flexible one compared to NCs. The greater transparency of CNPs than CNPp was postulated due to the formation of the densely packed order of intra-inter hydrogen bonds found in CNPs, which allowed more light to transmit through the film and reduce the light to scatter. In addition, the higher crystallinity with a smaller aspect ratio could also promote the higher transparency of CNPs to give the combination of influencing factors in explaining the level of transparency of CNP.

Keywords Cellulose nanopaper · Oil palm empty fruit bunch · Nanocellulose · Cellulose nanocrystals · Cellulose · Acid hydrolysis

✉ Athanasia Amanda Septevani
athanasia.amanda.septevani@brin.go.id

1   Research Center for Environmental and Clean Technology, National Research and Innovation Agency, Komplek BRIN Cisitu, Bandung 40135, Indonesia

2   Department of Chemical Engineering, Institut Teknologi Indonesia, Jl. Raya Puspiptek Serpong, South Tangerang 15314, Indonesia

3   Research Center for Biomass and Bioproducts, National Research and Innovation Agency, Jl. Raya Bogor Km 46 Cibinong, Bogor 16911, Indonesia

4   Research Center for Chemistry, National Research and Innovation Agency, Kawasan PUSPIPTEK Serpong, South Tangerang 15314, Indonesia

5   Research Center for Advanced Materials, National Research and Innovation Agency, Kawasan PUSPIPTEK Serpong, South Tangerang 15314, Indonesia

6   Research Center for Electronics, National Research and Innovation Agency, Komplek BRIN Cisitu, Bandung 40135, Indonesia

7   Eijkman Institute for Molecular Biology, Jakarta, Indonesia

Introduction

Paper is one of the most widely used materials in everyday life, from exchanging information through writing and printing to storage. Very recently, cellulose nanopaper (CNP), a new type of paper made of nanocellulose (NC), has attracted great attention as a promising substrate candidate for functionalized optical products in various potential applications due to its transparency and remarkably mechanical properties while maintaining the sustainability, and certainly its environmental friendliness [1–3]. CNP holds enormous applications, including LEDs, screens, solar cells, sensors, supercapacitors, UV blocking and paper-based anticounterfeiting [4, 5], with the market demand expected to be $73 billion in 2025 [6]. Compared to traditional paper with a 15 to 30 μm-wide cellulose fibers, CNP is made up of 3 to 15 nm wide nanocellulose (NC). It consists of densely packed NC which left no cavity for light scattering offering higher transparency and lower haze compared to its microscale paper [7]. The preparation process of CNP is similar to the traditional paper [8, 9]. The process includes the solvent

evaporation method [10, 11], drying of NC suspension into the repetitive rolling process [12], vacuum filtration [13], solvent casting [13], pressure filtration [14] and filtration accompanied with the hot pressing method [15, 16].

NC as the base material on CNP production can be distinguished into two types, known as cellulose nanofibers (CNF) and cellulose nanocrystals (CNC). CNF containing crystalline and amorphous cellulose are long, flexible, and strongly entangled networks of nanofibrils. It can be produced by high shearing forces [17], including direct mechanical fibrillation [18, 19], mechanical fibrillation after enzymatic hydrolysis [9, 20], mechanical fibrillation after 2,2,6,6-tetramethylpiperidine-1-oxyl radical (TEMPO)-mediated oxidation [21], and acid treatment [16]. Meanwhile, needle-like or rod-like- CNC, is generally produced by acid hydrolysis [22, 23]. CNC can be produced from strong acid hydrolysis, mostly using sulphuric acid (NCs) or mild acid hydrolysis by using phosphoric acid (NCp). NCs typically have a low aspect ratio, while highly aspect ratio of CNC is obtained from phosphoric acid hydrolysis. The crystallinity of NCs is higher than that of NCp at up to above 90% [24]; nevertheless, the higher thermal stability of fCNC is typically observed for NCp rather than NCs [25].

NC can be isolated from various lignocellulosic biomass[26]. Indonesia has a great advantage as the largest crude palm oil (CPO) producer in the world. A large amount of solid residue, including oil palm empty fruit bunch (OPEFB), has scarily been generated and discarded during palm oil production, leading to environmental problems. To overcome this problem while giving a value-added to transform this huge amount of biomass waste into highly innovative material, the utilization of OPEFB can be an alternative solution as the raw material-based NC for the production of CNP.

In this study, we aim to produce NC from OPEFB using different types of acid hydrolysis: strong acid and mild acid. The obtained NC-OPEFB was then used to produce OPEFB-based CNP. The structure–property relationship of different acid hydrolysis-based NC was systematically studied on the obtained CNP properties in terms of optical transparency, mechanical properties, and surface morphology. To the best of our knowledge, there is no study on the production of transparent CNP from OPEFB. This study investigated the potential use of OPEFB as a promising resource to produce CNP.

Material and method

Materials

OPEFB was obtained from Lampung, Indonesia. The OPEFB was chopped to 30 mesh and oven-dried until the moisture content is less than 10%. All chemicals, including NaOH, H_2O_2, H_2SO_4, and H_3PO_4 were technical grade-based chemicals.

Method

Pretreatment and bleaching

Pretreatment and bleaching were conducted before the preparation of NCs/NCp. Pretreatment was performed using a bench-scale reactor CHEMEX with a feed capacity of 500 g. Cyclone, belt press, washing tank, and buffer tank were equipped in the reactor. Dilute alkaline (NaOH 10%) was used as a solvent with a solid–liquid ratio of 1:5. The mixture was heated at 150 °C, 7–8 bar for 30 min. The treated OPEFB was neutralized with tap water and oven-dried until the moisture content was around 10%. The bleaching process was conducted by adding five grams of dried-treated OPEFB into 500 ml H_2O_2. The mixture was then agitated, heated, and kept at 80–85 °C for an hour. After finished, the cake was filtered and washed until neutral.

Preparation of nanocellulose (NCs and NCp) using acid hydrolysis

Preparation of NCs was conducted using 36% sulfuric acid with a solid/liquid ratio of 1:80 at different temperatures (50 °C, 60 °C, 70 °C) for 3.5 h denoted as NCs50, NCs60, and NCs70, respectively. The solution was then centrifuged at 10,000 rpm for 15 min to remove excess acid. Dialysis in aquadest was conducted for 3–4 days to neutralize the solution. Meanwhile, NCp was produced using phosphoric acid of 63% with solid/liquid ratio of 1:185 for 3.5 h at the temperature of 50 °C, 70 °C, 80 °C, 90 °C and were denoted as NCp50, NCp70, NCp80, and NCp90, respectively.

Characterization of nanocellulose

The morphological structure and elemental analysis of NC from OPEFB were analyzed using Scanning Electron Microscopy (SEM) on the gold-coated sample using the JEOL JSM-IT200 integrated Energy Dispersive X-ray Spectroscopy (EDS) operated at 5 kV in the Research Center for Physics-BRIN. At the nanoscale, the morphology of NC was analyzed by Transmission Electron Microscopy (TEM) at Eijkman Research Institute. The NC suspension was spotted onto a gold glider grid G400G and then stained with 2% aqueous uranyl acetate. The prepared samples were analyzed in a JEOL 1010 at 80 kV. Zeta potential analysis was characterized in aquadest with the ratio of sample:aquadest is 1:10 using Horiba Nano Partica SZ-100. The laser resource was DPSS laser with a wavelength of 532 nm and a laser angle of 173°. The analysis was done in automatic mode.

X-Ray analysis was conducted on a Shimadzu Maxima X-ray diffractometer (XRD-7000, Japan) generated at 40 kV and 30 mA. NC samples were nicely placed in the sample holder and scanned over a range of 2θ from 10° to 35° with a speed of 2 min^{-1}. To provide a clearer baseline, a blank sample was also run with the same condition presented except for the NC in the sample holder. The blank data was then subtracted from the data with the NC sample. The crystallinity index (CrI) was calculated using Segal's method as follows:

$$\%CrI = \frac{I(200) - I(amorphous)}{I(200)} x100\% \qquad (1)$$

where I(200) represents the intensity of crystallinity peak at the maximum 2θ between 22°–23°, and I(amorphous) is the minimum intensity at 2θ between 18°–19° (of the amorphous region).

Synthesis of cellulose nanopaper

NC with a varied concentration of solid content (Y %) at the range of 0.2% wt. − 0.7% wt. was ultrasonicated using Ultra-Sonica at 500 kW with an amplitude of 30% for 10 min. The mixture was then filtered using a Whatman filter grade 1 to remove remaining aggregates and agglomerated NC. The suspension was poured on Petri dishes and left for five days for drying at ambient temperature. CNP from blended Whatman filter paper No.1 was also fabricated with the same procedure for comparison as a micropaper. CNP derived from CNs was denoted as CNPsX-Y, while CNP derived from NCp was denoted as CNPpX-Y. X has represented the temperature process during hydrolysis of NC and Y is the concentration of NC in CNP.

Characterization of cellulose nanopaper

The CNP was characterized by its optical and mechanical properties. The optical properties of the CNP were measured using a UV–VIS Spectrophotometer from Ocean Optics (Maya 2000 PRO) using Whatman filter paper no 1 as blank reference material. The transmittance of the samples was measured between 400–1000 nm wavelengths. Tensile tests test was carried out using a Universal Testing Machine, Orientec UCT-5 T Japan, equipped with a 100 N load cell on the strips sample at size 6 mm × 25 mm. The testing speed was 2 mm min^{-1}. The average values with standard deviation were calculated based on a minimum of three measurements. All digital photos of CNP in this study were taken by a digital camera without any polarizer or filter.

Result and discussion

The first step to prepare NC is to isolate and increase cellulose purity from OPEFB by removing lignin and hemicellulose that bind the fibers together through pretreatment using alkaline (NaOH) followed by bleaching using H_2O_2. Hemicellulose and lignin removal represents a critical point during processing and in the final properties of NC and thus CNP. Hemicellulose hinders the formation of strong hydrogen bonds between crystalline by physically inhibiting direct contact between NC. Moreover, hemicellulose is a highly plasticizer by absorbing moisture causing a decrease in cohesion. Accordingly, the lower content of hemicellulose is preferred as it can improve the mechanical properties of CNP [27]. Meanwhile, the presence of lignin produces darker films and provides undesired physical, optical, and water interaction properties of CNP [28]. The removal of lignin and hemicellulose is also reported to increase defibrillation resulting in a large number of single fiber [29]

In this study, cellulose from OPEFB was successfully isolated via our previously reported protocol using the simultaneous pretreatment process at the purity of $84.03 \pm 0.3\%$ of cellulose, and $12.6 \pm 0.1\%$ of hemicellulose, and $3.1 \pm 0.2\%$ of lignin. The result was higher in terms of all three components than the cellulose standard [30, 31].

The properties of nanocellulose using different types of acid hydrolysis

Stability of nanocellulose

The preparation of NC was conducted via two types of acid hydrolysis, namely (i) strong acid hydrolysis using sulphuric acid (NCs), and (ii) mild acid hydrolysis using phosphoric acid (NCp). A stabilization test was conducted to simply confirm the formation of NC. The dispersion stability of NCs and NCp at various temperatures (Fig. S1 and Fig S2, respectively in the Supplementary Data) was physically observed by taking the photographs for up to two weeks. Stable and transparent suspensions were observed in all NCs samples while a stable dispersion of NCp was observed at temperature ≥ 70 °C. NCp at 50 °C showed the formation of two-phase after 1 h. NCs exhibits higher stability and transparency than NCp. This difference might be ascribed to the presence of a relatively large NCp bundle and network which scattered the light as well as physical entanglement between the fibers from the network [22]. The stability of nanocellulose dispersion can also be quantitatively investigated by zeta potential

Table 1 Shows the zeta potential of NCs and NCp processed at different temperatures

Sulfuric acid hydrolysis		Phosphoric acid hydrolysis	
Samples	Zeta potential (mV)	Samples	Zeta potential (mV)
NCs50	− 42.37 ± 0.15	NCp50	− 17.6 ± 0.30
NCs60	− 51.3 ± 0.10	NCp70	− 43.4 ± 0.36
NCs70	− 54.5 ± 0.17	NCp80	− 45.43 ± 0.15

(Table 1). The greater stability of nanocellulose can be attributed to a higher surface charge across the electric field due to the presence of a negative surface charge on the surface of nanocellulose.

Typically, the zeta potential value at 30 mV represents the onset of stabilization of fibril dispersion, in which this zeta potential value above the onset value indicates a stable dispersion of nanomaterials [32]. As reflected by the storage stability test for up to 2 weeks (Supplementary Data), samples of NCs at all diffrent temperatures exhibited zeta potential above 40 mV showed the greater dispersion stability, while only NCp processed at the temperature above 70 °C showed the good storage stability in agreement to a higher zeta potential at about 40 mV.

Further, the yellow-brownish suspension observed in the phosphoric acid hydrolysis at 90 °C due to over hydrolysis exceeded the formation of glucose and was further dehydrated into carbon thus the analysis of zeta potential was not performed. Dong et al. (1998) reported that at a high temperature above 70 °C, side reactions such as dehydration reactions can start to occur leading to the color change from yellowish to black as a result of carbon formation. The formation of carbon can influence the storage stability of the suspension as supported by the two phase's formation of NCp90 after 1 day (Fig. S2 in the Supplementary Data).

Morphology studies of nanocellulose

Figure 1 shows SEM images of NCs at different temperatures of hydrolysis. The dimension of NCs50 was measured at 502 ± 342 nm in diameter (Fig. 1A), while the dimensions of NCS60 (Fig. 1B) and NCS70 (Fig. 1C) were very small and so difficult to be measured. This result revealed that the increase in hydrolysis temperature significantly decreased the size of the fiber. To determine
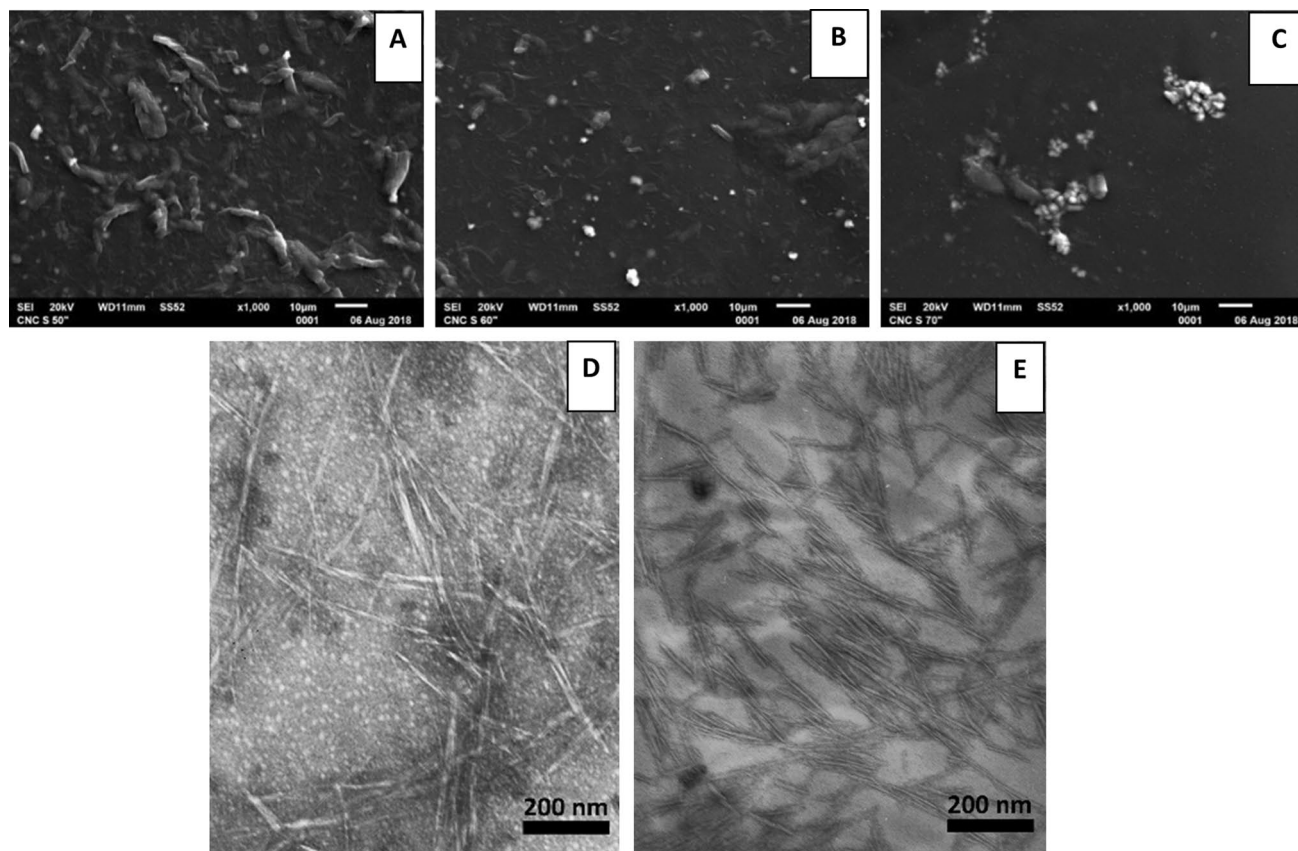
Fig. 1 SEM analysis of NC from sulphuric acid hydrolysis at **A** 50 °C, **B** 60 °C, and **C** 70 °C as well as TEM analysis of NC from sulphuric acid hydrolysis at **D** 60 °C, and **E** 70 °C

the dimension of cellulose at the nanoscale, TEM analysis was further conducted for NCs60 (Fig. 1D) and NCs70 (Fig. 1E). Rod-like CNC was observed from acid hydrolysis at 60 °C (NCs60) with a length of 132 ± 22 nm and diameter of 9 ± 4 nm, while NCs70 has a length of 108 ± 9 nm and diameter of 8 ± 1 nm. The dimension of this NC was smaller than reported standard cotton NC from Whatman filter paper (169 ± 49 nm in length and 11 ± 3 nm, in diameter) [33].

Morphology and size dimensions of cellulose nanofiber (NCp) from phosphoric acid hydrolysis were analyzed using SEM as illustrated in Fig. 2. The increasing temperature significantly affected the dimension of obtained NC, indicating that the temperature plays a key role in controlling the dimension of nanocellulose. Nevertheless, the temperature should be controlled, at which dehydration have to be avoided. NCp50 had a diameter of 847 ± 346 nm and a length in micron-scale (Fig. 2A). The measurement of the microscale length was difficult as the fibers were tangled with each other with no distinctive endpoint. At 70 °C, the diameter became much smaller, which was at 492 ± 188 nm. Meanwhile, the dimension of NCp80 could not be measured based on SEM, and thus, TEM was used for the investigation (Fig. 2E).

TEM micrograph of NCp80 in Fig. 2E revealed the formation of NC in the length of about 395 ± 28 nm and diameter of 10 ± 3 nm, which was a distinctively higher aspect ratio than NCs (Fig. 1D). It was reported that sulfuric acid is known as a very strong hydrolytic agent that is very aggressive in attacking amorphous regions and thus produces NC with a short nano-sized dimension compared to mild acid and even other strong acids such as hydrochloric acid [34].

## Chemical structure and composition of nanocellulose

As previously discussed, during the acid hydrolysis process, the acid could aggressively attack the disorder or amorphous fraction of cellulose including hemicelluloses and lignin, while the crystalline region is maintained due to its higher resistance to acid disorder [35]. Based on component analysis of nanocellulose (after the hydrolysis), there was an increase in cellulose content and reduce in hemicellulose and lignin content, compared to microcellulose (before hydrolysis). NCs is composed of $89.5 \pm 0.6\%$ of cellulose, $8.4 \pm 0.4\%$ of hemicellulose and $2.1 \pm 0.2\%$ of lignin, while NCp is composed of $89.0 \pm 3.09\%$ of cellulose, $8.9 \pm 2.4\%$ of hemicellulose and $2.2 \pm 0.7\%$ of lignin.

FTIR spectroscopy has been also extensively used in cellulose research since it presents a relatively easy method of obtaining direct information on chemical changes during various chemical treatments including acid hydrolysis. In the FTIR analysis, the spectra of bleached treated raw EFB (microcellulose), the sulfuric acid hydrolyzed of cellulose (NCs), and the phosphoric acid hydrolyzed cellulose (NCp), are shown in Fig. 3.

The peaks around 2892–2904 cm^{-1} indicate the aliphatic saturated C-H stretching associated with methylene groups in cellulose, hemicellulose, and lignin [36, 37]. The absorption peaks in the region of 1342–1305 cm^{-1} corresponded to the CH$_2$ rocking of polysaccharides [38–40]. All spectra
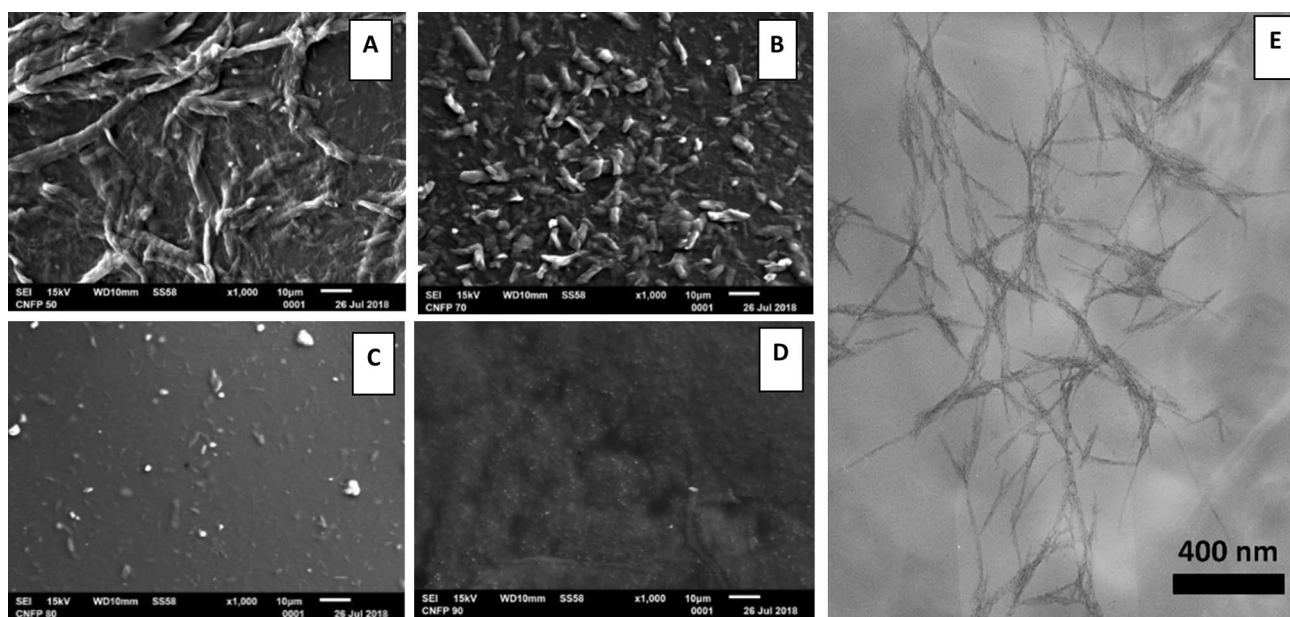

Fig. 2 SEM analysis of NC from phosphoric acid hydrolysis at **A** 50 °C, **B** 70 °C, **C** 80 °C, **D** 90 °C as well as TEM analysis of NC from phosphoric acid hydrolysis at **E** 80 °C
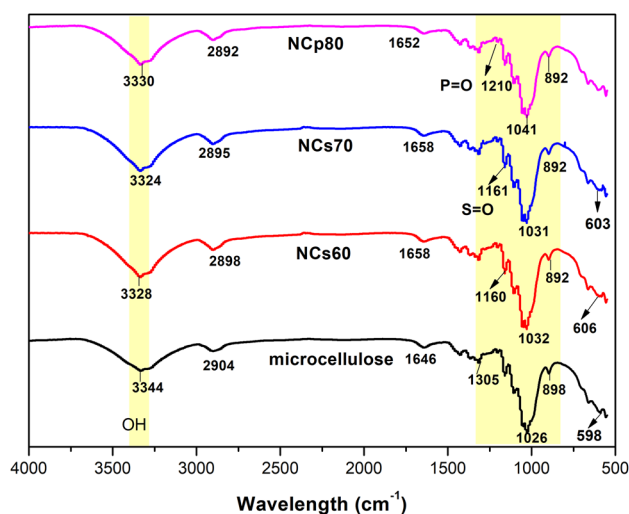
Fig. 3 FTIR spectra of microcellulose and nanocellulose

Fig. 4 X-Ray Diffraction of nanocellulose

are dominated by the peaks of hydroxyl groups (OH) indicating the hydrophilic cellulose. The distinction between NCs, NCp, and micropaper in the case of the hydroxyl group exhibited OH spectra shifting for the samples before and after hydrolysis. The OH stretching peak of the NCp shifted from 3344 cm^{-1} before hydrolyzed to 3330 cm^{-1}. Similarly, NCs before hydrolysis showed OH spectra shifted from 3344 to 3328 cm^{-1}. The difference between hydrolyzed samples and unhydrolyzed samples could also be investigated from the spectra shifting from 2904 cm^{-1} (micropaper) to 2892 cm^{-1} for NCp, also the peak of 2898 cm^{-1} for NCs60 and 2893 cm^{-1} for NCs70. There is also shifting spectra from 898 cm^{-1} before hydrolyzed to 892 cm^{-1} after treatment; these are the evidence of the cleavage of a glycosidic bond to break a long chain of cellulose into nanocrystallite because of hydrolysis [38, 40–43].

Further, the peak at 1161 cm^{-1} in the NCs spectrum corresponds to the presence of sulfonate group (SO$_2$) and 603–606 (SO$_2$ scissoring) cm^{-1} are observed for NCs70 and NCs60 compared to micropaper [34, 38, 44]. The unhydrolyzed sample was shifted from 598 to 603–606 cm^{-1}. This result indicated that the sulfonate group was successfully attached to the NC structure. In terms of the presence of the phosphate group in NCp, although a new peak of the vibrations band of P=O occurred at 1210 cm^{-1} and the vibrations band of P–O–Alkyl stretching was observed at 1041 cm^{-1}, P–OH stretching at 916 cm^{-1} was not clearly revealed [45]. This may indicate minor phosphate group functionalization on the surface of the NCp structure. It was reported that the sulfonyl has greater ionic attachment than phosphoryl ion sites, as reflected by its higher dispersion ability [39, 46] as a noted by the higher zeta potential of NCs compared to NCp and attributed to the agglomeration that occurs on the surface of the phosphate from SEM micrographs of CNP
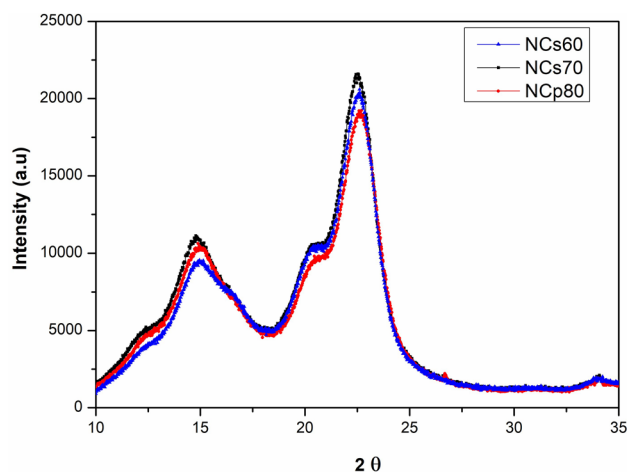
in the following discussion. Finally, the elemental analysis using SEM–EDS (Fig. S3 in the Supplementary Data) confirmed that the presence of phosphorous was not detected in NCp while at about 0.01 ± 0.01% mass of sulfur element was detected in NCs.

Crystallinity of the nanocellulose

It is known that cellulose contains both crystalline and amorphous regions in molecular structure. The presence of acid will selectively attack the disordered (amorphous) region. At the same time, the highly ordered and arranged (crystalline) structure remains stable in an acid condition, leading to the increasing crystallinity index. The degree of crystallinity of the obtained NC was investigated on the selected NC of NCs60, NCs70 and NCp80 (Fig. 4) by using X-Ray Diffractometer and the determination of crystallinity index (CrI, %) was calculated by using the Segal method. This method has been widely used in the crystallinity study of cellulose as represented in Eq. (1).

Based on the Segal method, the degree of crystallinity of NCs60, NCs70, and NCp80 is 77.1%, 76.1%, and 74.7%, respectively. Sulphuric acid hydrolysis has been known as a promising method to produce higher crystalline NC because the presence of strong acid could aggressively attack the disorder or amorphous region rather than other mild acids. As expected, the crystallinity of NCs60 and NCs70 were higher than NCp80. The crystallinity of OPEFB-NC in this work also showed similar results to the study on palm biomass-based NC from palm mesocarp fiber using a similar method at 75–77.8% [38]. At the same resources of OPEFB, the crystallinity of the obtained NC from acid hydrolysis both sulphuric and phosphoric acid also shows a higher crystallinity compared to that of OPEFB-NC obtained from chemo-mechanical via High-Pressure Homogenizer with

the maximum crystallinity at 69% [47], suggesting acid hydrolysis offers a promising method to produce a higher crystallinity.

The structure–property relationship of cellulose nanopaper associated with different types of nanocellulose

Prior to the fabrication of CNP via dry-casting, previously obtained NCs and NCp were subsequently filtered using Whatman filter paper grade 1 to remove unreacted aggregate and agglomerated NC as this contaminant was detected in microscopy analysis (Figs. 1 and 2). During the dry-casting, the formation of thin-film CNP occurs when the fibrils are connected to each other and formed inter-intra connection hydrogen bonding along with the increasing concentration of NC due to the evaporation of the water [27]. In some cases, a dry-casting method was preferred for the preparation of CNP for the high viscosity of nanocellulose suspension [7]. Figures 5 and 6 show the visual photography of CNPs from $NC_S(s)$ and CNPp from NCp at different concentrations.

In terms of the effect of NC concentration, reduced transparency of CNP was observed by the increasing concentration of NC_S. However, it should be taken into account that the low concentration reduced the mechanical properties of CNP as the thickness of the CNP reduced accordingly, leading to a lower mechanical strength. Physically observed in both transparency and mechanical strength, the best CNP was obtained from NCs60 and NCs70, due to the greater interconnection of hydrogen bonding between nanoscale cellulose.

Figure 6 displays CNP from NCp at different concentration (0.2% wt., 0.3% wt. and 0.4% wt.). Similar to CNPs, the dimension and concentration greatly affected the transparency of CNPp. As expected, CNPp50 produce an opaque white paper that was visually similar to conventional micro-paper due to the micro size diameter of NCp50 at almost 1 μm (Fig. 2).

Meanwhile, CNPp70 and CNPp80 exhibited better transparency than CNPp50, which was attributed to the significantly smaller dimension of NCp in the formulation. Nevertheless, the transparency of CNPp was lower than that of CNPs for all formulations. In the dispersion, longer entanglement of NCp tends to form non-homogeneous dispersion, which hindered the ordered tight packing between inter-intra hydroxyl groups on the surface of nanofibers and thus decreases the transparency of CNP [7].

Fig. 5 CNP made of NCs from sulphuric acid hydrolysis at different temperatures and concentrations
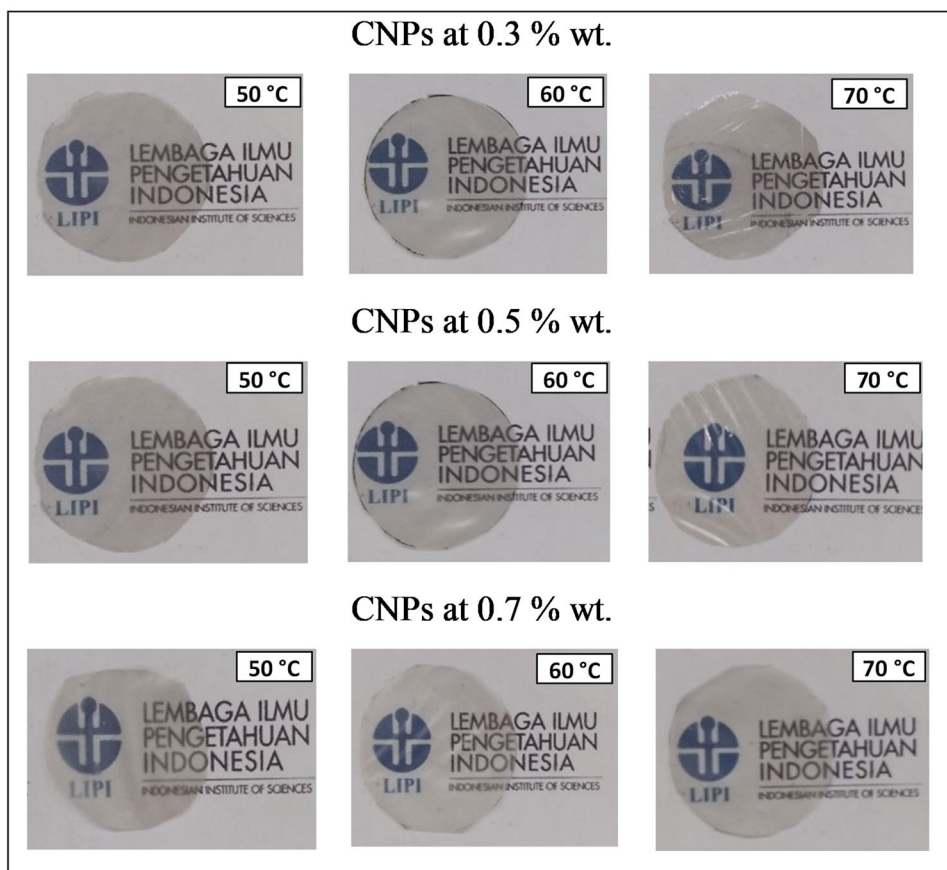
**Fig. 6** CNP made of NCp from phosphoric acid hydrolysis at different temperatures and concentrations
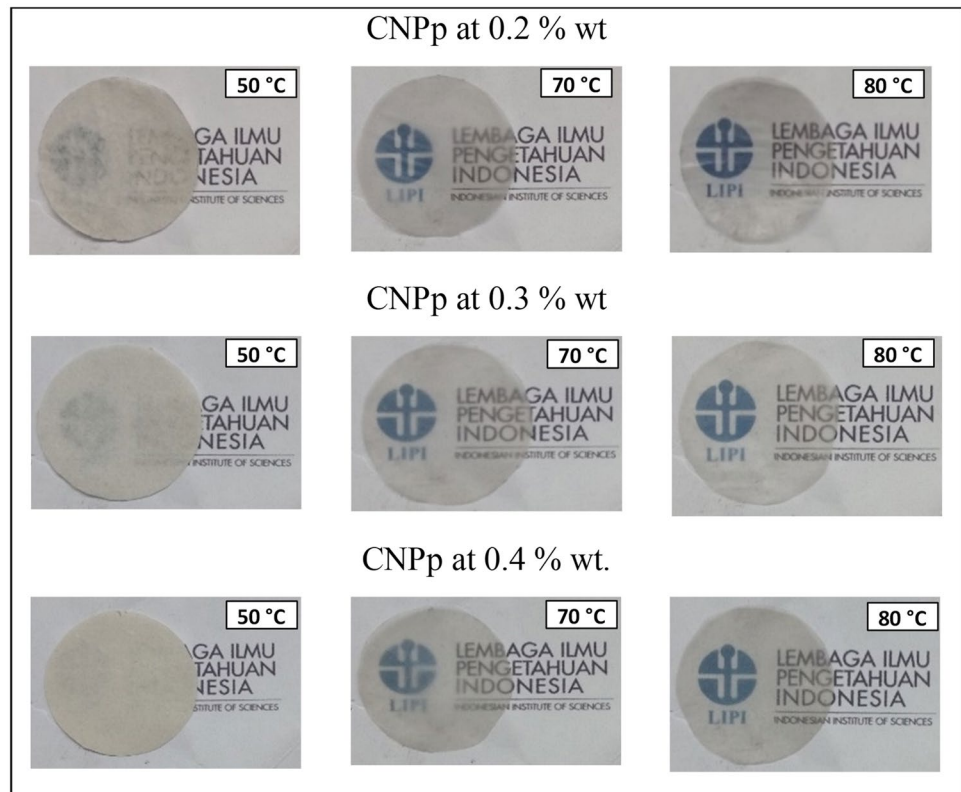
Optical properties of the CNP

The optical properties of CNP are critical parameters for the application of CNP as a substrate in optoelectronics [48]. The optical properties of CNP are investigated by determining the regular light transmittance with a UV–visible spectrometer in the wavelength of between 400 and 800 nm [49]. Wavelength versus transmittance for both CNPs and CNPp are represented in Fig. 7.

CNPs70-0.5 and CNPs70-0.3 exhibited the highest transmittance at a maximum of 65% among other formulations of NCs at different temperatures and concentrations. Meanwhile, the increase of NCs concentration to 0.7% wt. (CNPs70-0.7) reduced the maximum transmittance to 40%, which simply was attributed to an increase in thickness, thus reducing the intensity of the visible light to pass through the substrate in comparison to other studies on the production of CNP from biomass waste, the maximum transparency of CNP made of OPEFB-NCs in this study was similar to that of CNP from wood flour-NC at about maximum 60% transmittance, suggesting the EFB as a promising source of CNP [50].

In general, the transparency of CNPs was higher than that of CNPp. For example, the highest transparency of CNPp was only achieved at 30% transmittance for CNPp80 at 0.2%, while the transparency of other CNPp was lower than 20% transmittance. The opaqueness and lower transparency of the
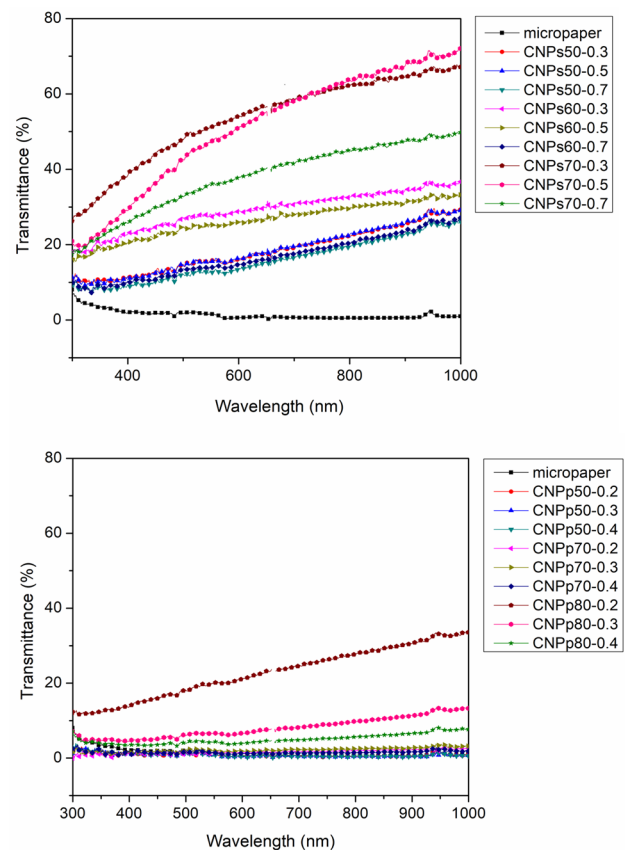
Fig. 7 Transparency of CNPs (upper) and CNPp (below)

Fig. 8 **A**. Intra and inter molecular hydrogen bonds of NC in CNP; **B**. schematic illustration of light transmission in CNP associated with different types of nanocellulose
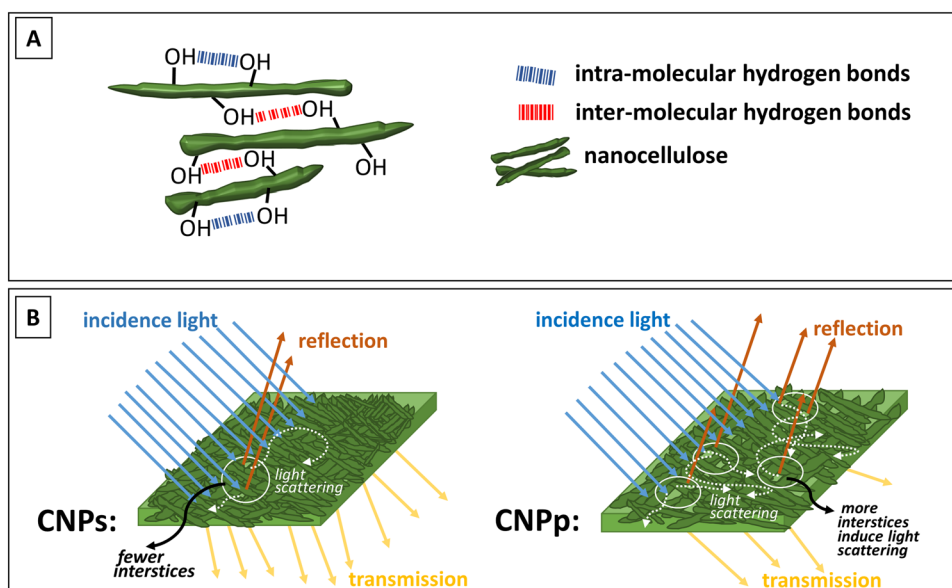
CNPp compared to CNPs might be also attributed to several factors. The common explanation is first, associated with the formation of the densely packed order of intra-inter hydrogen bond between NC in CNP, which allows more incidence of light to transmit the light through the film and reduces the light to scatter [48]. As illustrated in Fig. 8a, the electrostatic attractions between oxygen and hydrogen atoms of the adjacent ring in the individual cellulose nanofibril, induce intra-molecular hydrogen bonding leading to more stabilized glycosidic linkages and linear chain configuration. In addition, the inter-chain hydrogen bonds between the adjacent polymeric cellulose nanofibrils promote parallel stacking to further create densely packed and firmed cellulose structures into microscale predecessors, in this case, is nanopaper.

Figure 9 shows the SEM images of the obtaining CNP after drying for selected CNPs and CNPp. The well-dispersed of individual NCs as reflected in Fig. 1E could be densely and uniformly packed during the casting process (Fig. 9, upper). Thus, the interstices between fibers could be eliminated to avoid light scattering (as illustrated in Fig. 8b), leading to higher transparency of CNPs. In contrast, NCp, as reflected by Fig. 2E promoted the agglomerated fibers and voids in the sheet and thus creating more interstitial cavities (Fig. 9, below) resulting in a more incidence of light to scatter (Fig. 8b) and thus lower % transmittance, meaning low optically transparent paper was obtained [51]. Residual sulphate groups (SO_4^{2-}) were also reported to provide negative charges which offered a better dispersibility of NCs compared to other types of acids, in this case, phosphoryl as reflected by FTIR spectra (Fig. 3). Finally, crystallinity was also reported to affect transparency [7, 27, 52]. CrI of NCs60 and NCs70 was higher than NCp80 leading to the higher transparency of CNP made of NCs (Fig. 4). Hence,

it is postulated that the combination of influencing factors in explaining the level of transparency of CNP was attributed to the characteristics of the NC as a result of the temperature and type of acid variables.

Mechanical properties of CNP

Mechanical properties of CNP can be affected by several factors, including lignin content, the inter-fibrillary hydrogen bonds within NC, geometry, and crystallinity. Selected samples were prepared as representative of the control types of NCs and NCp (Table 2).

CNP derived from OPEFB exhibited good mechanical properties compared to the conventional micropaper (Whatman No.1). Lignin is reported to hinder hydrogen bonding and thus causes a reduction in the mechanical strength [53], but in this study, all the lignin content was maintained at the same level as the sources of cellulose come from the same batch of treated OPEFB. The size of NC also has an important impact on the mechanical properties of CNP. It was expected that the smaller diameter led to a stronger CNP [53]. Nevertheless, the crystallinity of cellulose is also crucial to its mechanical and thermal properties [27]. Amorphous regions were eliminated due to the presence of strong acid resulting in stiffer and higher crystalline NCs compared to NCp (Fig. 4).

Hence, although the aspect ratio of NCs was lower than that of NCp, thus leading to greater transparency, the tensile strength of CNPp is stronger than CNPs, which was attributed to flexible and longer fibrils in combination with lower crystallinity [11, 54]. It is also reported that a high aspect ratio of NC-based CNP is mostly selected compared to NCs based CNP as flexible printed electronics [6]. Further,
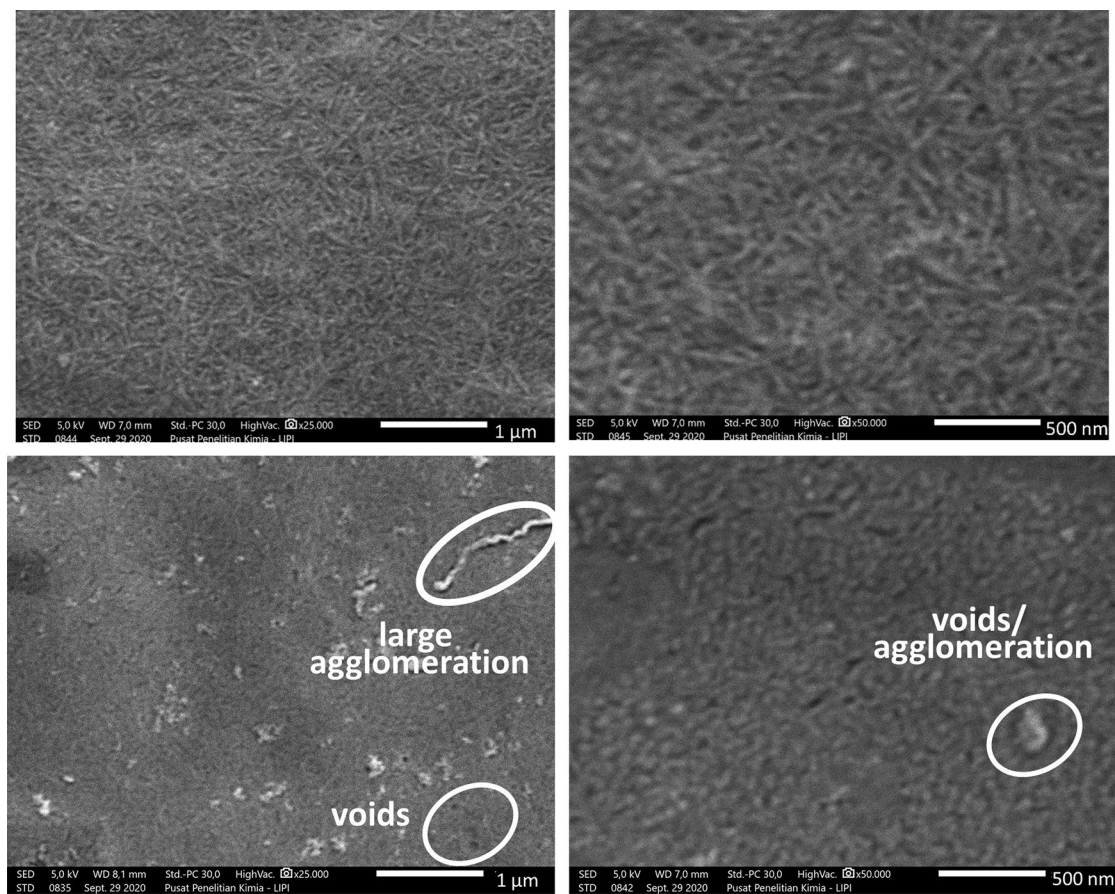
Fig. 9 SEM of CNPs (upper) and CNPp (below) sheet

Table 2 Mechanical properties of CNPs and CNPp

Sample	Tensile strength (MPa)	Improvement%	Young's modulus (MPa)	Improvement%
Micropaper	1.33 ± 0.09	–	109.22 ± 12.50	–
CNPs50	1.51 ± 0.74	13.53	146.62 ± 19.96	34.24
CNPs60	2.19 ± 0.22	64.66	265.99 ± 92.65	143.54
CNPs70	3.46 ± 0.32	160.15	302.98 ± 152.89	177.40
CNPp50	1.61 ± 0.15	21.05	156.84 ± 22.04	43.60
CNPp70	3.18 ± 0.24	139.10	270.62 ± 9.42	147.78
CNPp80	3.60 ± 0.40	170.67	331.97 ± 70.39	239.49

CNPp exhibited higher tensile strength compared to CNPs was might be attributed to the absence of an interconnected fibrillar network in the NCs network as supported by SEM images of a web-like structure of NCp (Fig. 2) which was reported as the factor to increase tensile strength [55].

Table 2 shows that the improvement of the tensile strength of CNPs and CNPp compared to micropaper was achieved at 160% and 171%, respectively. In fact, the tensile strength of the obtained CNP is typically lower than other reported nanopaper, which might be attributed to the presence of an inorganic contaminant, in this case, is silica at 0.28–0.34% mass,

originally coming from OPEFB as reflected by SEM–EDS results (Table S1 in the Supplementary Data). According to Amiralian et al. (2015) [56] these inorganic particles could interfere with the inter-intra molecular hydrogen bonding between the nanocellulose and act as ''stress raisers'', which could adversely affect the strength of the sheet. Nevertheless, it was also observed that the greater improvement on the young modulus for CNPp was double than that of control micropaper indicating that the CNP developed from OPEFB showed promising load-bearing characteristics compared to the microscale paper.

Conclusion

CNP was successfully produced from NC derived from oil palm empty fruit bunch (OPEFB) via sulphuric acid (NCs) and phosphoric acid (NCp) hydrolysis. The CNP showed outstanding performance regarding its optical properties, with the highest transmittance of ~70% for CNPs and 200% in improved mechanical properties for CNPp than conventional micropaper. Temperature and types of acid were found to have a significant role in affecting the dimension of the NC, which determines its morphology and crystallinity. A smaller aspect ratio with higher crystallinity was observed from CNPs, resulting in greater transparency than CNPp and conventional micropaper. On the other hand, a higher aspect ratio and lower crystallinity benefited CNPp in terms of high tensile strength. In summary, the obtained CNP demonstrated distinctive effects based on different NC (NCs and NCp), suggesting that the fabrication of CNP can be controlled to meet the requirement for various applications.

Declarations

Conflict of interest The authors have no relevant financial or non-financial interests to disclose.

References

1. Ha D, Fang Z, Zhitenev NB (2018) Paper in electronic and optoelectronic devices. Adv Electron Mater 1700593:1–20. https://doi.org/10.1002/aelm.201700593
2. Zhang Z et al (2019) Cellulose nanopaper with controllable optical haze and high efficiency ultraviolet blocking for flexible optoelectronics. Cellulose 26(4):2201–2208. https://doi.org/10.1007/s10570-019-02253-y
3. Septevani AA, Burhani D, Sampora Y (2022) Nanocellulose Materials: Fabrication and Industrial Applications. In: Oraon R, Rawtani D (eds) Nanocellulose in electronics and electrical industry. Elsevier, Amsterdam, pp 217–246. https://doi.org/10.1016/B978-0-12-823963-6.00010-7
4. Chang H et al (2020) Flexible, transparent, and hazy cellulose nanopaper with efficient near-infrared luminescence fabricated by 2D lanthanide (Ln = Nd, Yb, or Er) metal-organic-framework-grafted oxidized cellulose nanofibrils. Inorg Chem 59(22):16611–16621. https://doi.org/10.1021/acs.inorgchem.0c02518
5. Li X, Zhang X, Yao S, Chang H, Wang Y, Zhang Z (2020) UV-blocking, transparent and hazy cellulose nanopaper with superior strength based on varied components of poplar mechanical pulp. Cellulose 27(11):6563–6576. https://doi.org/10.1007/s10570-020-03236-0
6. Hoeng F, Denneulin A, Bras J (2016) Use of nanocellulose in printed electronics: a review. Nanoscale 8(27):13131–13154. https://doi.org/10.1039/c6nr03054h
7. Isobe N, Kasuga T, Nogi M (2018) Clear transparent cellulose nanopaper prepared from a concentrated dispersion by high-humidity drying. RSC Adv 8(4):1833–1837. https://doi.org/10.1039/c7ra12672g
8. Mtibe A, Linganiso LZ, Mathew AP, Oksman K, John MJ, Andjiwala RD (2015) A comparative study on properties of micro and nanopapers produced from cellulose and cellulose nanofibers. Carbohydr Polym 118:1–8. https://doi.org/10.1016/j.carbpol.2014.10.007
9. Henriksson M, Berglund LA, Isaksson P, Lindstro T (2008) Cellulose nanopaper structures of high toughness. Biomacromolecules 9(6):1579–1585
10. Wu Q et al (2013) Influence of temperature and humidity on nanomechanical properties of cellulose nanocrystal films made from switchgrass and cotton. Ind Crop Prod 48:28–35. https://doi.org/10.1016/j.indcrop.2013.03.032
11. Fukuzumi H, Saito T, Isogai A (2012) Influence of TEMPO-oxidized cellulose nanofibril length on film properties. Carbohydr Polym 93(1):171–177. https://doi.org/10.1016/j.carbpol.2012.04.069
12. Sehaqui H, Zimmermann T, Tingaut P (2014) Hydrophobic cellulose nanopaper through a mild esterification procedure. Cellulose 21:367–382. https://doi.org/10.1007/s10570-013-0110-5
13. Sehaqui H, Liu A, Zhou Q, Berglund LA (2010) Fast preparation procedure for large, flat cellulose and cellulose / inorganic nanopaper structures. Biomacromolecules 11:2195–2198. https://doi.org/10.1021/bm100490s
14. Osterberg M et al (2013) A fast method to produce strong NFC films as a platform for barrier and functional materials. Appl Mater Interfaces 5:4640–4647. https://doi.org/10.1021/am401046x
15. Missoum K, Martoïa F, Belgacem MN, Bras J (2013) Effect of chemically modified nanofibrillated cellulose addition on the properties of fiber-based materials. Ind Crop Prod 48:98–105. https://doi.org/10.1016/j.indcrop.2013.04.013
16. Wang H, Li D, Zhang R (2013) Preparation of ultralong cellulose nanofibers and optically transparent nanopapers derived from

waste corrugated paper pulp. BioResources 8(1):1374–1384. https://doi.org/10.15376/biores.8.1.1374-1384

17. Nechyporchuk O, Belgacem MN, Bras J (2016) Production of cellulose nanofibrils: a review of recent advances. Ind Crop Prod 93:2–25. https://doi.org/10.1016/j.indcrop.2016.02.016

18. Zhu H, Hu L, Cumings J, Huang J, Chen Y (2013) Highly transparent and flexible nanopaper transistor. ACS Nano 7(3):2106–2113. https://doi.org/10.1021/nn304407r

19. Wang QQ, Zhu JY, Gleisner R, Kuster TA, Baxa U, McNeil SE (2012) Morphological development of cellulose fibrils of a bleached eucalyptus pulp by mechanical fibrillation. Cellulose 19(5):1631–1643. https://doi.org/10.1007/s10570-012-9745-x

20. Wang W, Mozuch MD, Sabo RC, Kersten P, Zhu JY, Jin Y (2015) Production of cellulose nanofibrils from bleached eucalyptus fibers by hyperthermostable endoglucanase treatment and subsequent microfluidization. Cellulose 22(1):351–361. https://doi.org/10.1007/s10570-014-0465-2

21. Fukuzumi H, Saito T, Iwata T, Kumamoto Y, Isogai A (2009) Transparent and high gas barrier films of cellulose nanofibers prepared by TEMPO-mediated oxidation. Biomacromolecules 10(1):162–165. https://doi.org/10.1021/bm801065u

22. Xu X et al (2016) Highly transparent, low-haze, hybrid cellulose nanopaper as electrodes for flexible electronics. Nanoscale 8:12294–12306. https://doi.org/10.1039/c6nr02245f

23. Septevani AA et al (2018) Atomic layer deposition of metal oxide on nanocellulose for enabling microscopic characterization of polymer nanocomposites. Small 14(46):1803439. https://doi.org/10.1002/smll.201803439

24. Septevani AA et al (2019) The effect of acid hydrolysis treatment on the production of nanocellulose based on oil palm empty fruit bunches. J Kim Terap Indones 21(1):31–37. https://doi.org/10.14203/jkti.v21i1.416

25. Espinosa SC, Kuhnt T, Foster EJ, Weder C (2013) Isolation of thermally stable cellulose nanocrystals by phosphoric acid hydrolysis. Biomacromolecules 14:1223–1230. https://doi.org/10.1021/bm400219u

26. Lubis R, Wirjosentono B, Eddyanto, Septevani AA (2020) Preparation, characterization and antimicrobial activity of grafted cellulose fiber from durian rind waste. Colloids Surfaces A Physicochem Eng Asp 604:125311. https://doi.org/10.1016/j.colsurfa.2020.125311

27. Benítez AJ, Walther A (2017) Cellulose nanofibril nanopapers and bioinspired nanocomposites: a review to understand the mechanical property space. J Mater Chem A 5(31):16003–16024. https://doi.org/10.1039/c7ta02006f

28. Ferrer A et al (2012) Effect of residual lignin and heteropolysaccharides in nanofibrillar cellulose and nanopaper from wood fibers. Cellulose 19(6):2179–2193. https://doi.org/10.1007/s10570-012-9788-z

29. García-garcía D, Balart R, Lopez-Martinez J, Ek M, Moriana R (2018) Optimizing the yield and physico-chemical properties of pine cone cellulose nanocrystals by different hydrolysis time. Cellulose 25:2925–2938. https://doi.org/10.1007/s10570-018-1760-0

30. Burhani D, Septevani AA (2018) Isolation of nanocellulose from oil palm empty fruit bunches using strong acid hydrolysis. AIP Conf Proc 2024:020005. https://doi.org/10.1063/1.5064291

31. Septevani AA, Burhani D, Sudiyarmanto S (2018) Pengaruh Proses Pemutihan Multi Tahap Serat Selulosa dari Limbah Tandan Kosong Kelapa Sawit. J Kim Kemasan 40(2):71–78. https://doi.org/10.24817/jkk.v40i2.3508

32. Yang X et al (2017) Effects of preparation methods on the morphology and properties of nanocellulose (NC) extracted from corn husk. Ind Crop Prod 109:241–247. https://doi.org/10.1016/j.indcrop.2017.08.032

33. Septevani AA, Annamalai PK, Martin DJ (2017) Synthesis and characterization of cellulose nanocrystals as reinforcing agent in solely palm based polyurethane foam. AIP Conf Proc 1904:020042. https://doi.org/10.1063/1.5011899

34. Septevani AA et al (2020) Oil palm empty fruit bunch-based nanocellulose as a super-adsorbent for water remediation. Carbohydr Polym 229:115433. https://doi.org/10.1016/j.carbpol.2019.115433

35. Khawas P, Das AJ, Deka SC (2016) Production of renewable cellulose nanopaper from culinary banana (Musa ABB) peel and its characterization. Ind Crop Prod 86:102–112. https://doi.org/10.1016/j.indcrop.2016.03.028

36. Fahma F, Iwamoto S, Hori N, Iwata T, Takemura A (2010) Isolation, preparation, and characterization of nanofibers from oil palm empty-fruit-bunch (OPEFB). Cellulose 17(5):977–985. https://doi.org/10.1007/s10570-010-9436-4

37. Liu C et al (2016) Properties of nanocellulose isolated from corncob residue using sulfuric acid, formic acid, oxidative and mechanical methods. Carbohydr Polym 151:716–724

38. Chieng B, Lee S, Ibrahim N, Then Y, Loo Y (2017) Isolation and characterization of cellulose nanocrystals from oil palm mesocarp fiber. Polymers (Basel) 9(8):355. https://doi.org/10.3390/polym9080355

39. Phanthong P, Guan G, Ma Y, Hao X, Abudula A (2016) Effect of ball milling on the production of nanocellulose using mild acid hydrolysis method. J Taiwan Inst Chem Eng 60:617–622. https://doi.org/10.1016/j.jtice.2015.11.001

40. Haafiz MKM, Hassan A, Zakaria Z, Inuwa IM (2014) Isolation and characterization of cellulose nanowhiskers from oil palm biomass microcrystalline cellulose. Carbohydr Polym 103(1):119–125. https://doi.org/10.1016/j.carbpol.2013.11.055

41. Mandal A, Chakrabarty D (2011) Isolation of nanocellulose from waste sugarcane bagasse (SCB) and its characterization. Carbohydr Polym 86(3):1291–1299. https://doi.org/10.1016/j.carbpol.2011.06.030

42. Jiang F, Lo Hsieh Y (2013) Chemically and mechanically isolated nanocellulose and their self-assembled structures. Carbohydr Polym 95(1):32–40. https://doi.org/10.1016/j.carbpol.2013.02.022

43. Lamaming J, Hashim R, Leh CP, Sulaiman O, Sugimoto T, Nasir M (2015) Isolation and characterization of cellulose nanocrystals from parenchyma and vascular bundle of oil palm trunk (Elaeis guineensis). Carbohydr Polym 134:534–540. https://doi.org/10.1016/j.carbpol.2015.08.017

44. Souza NF, Pinheiro JA, Brígida AIS, Morais JPS, de sá Moreira M, de Souza F, de Freitas RM (2016) Fibrous residues of palm oil as a source of green chemical building blocks. Ind Crops Prod 94:480–489. https://doi.org/10.1016/j.indcrop.2016.09.012

45. Petreus T et al (2014) Preparation and cytocompatibility evaluation for hydrosoluble phosphorous acid-derivatized cellulose as tissue engineering scaffold material. J Mater Sci Mater Med 25(4):1115–1127. https://doi.org/10.1007/s10856-014-5146-z

46. Moon RJ, Martini A, Nairn J, Simonsen J, Youngblood J (2011) Cellulose nanomaterials review: structure, properties and nanocomposites. Chem Soc Rev 40:3941–3994. https://doi.org/10.1039/C0CS00108B

47. Jonoobi M, Khazaeian A, Tahir PM, Azry SS, Oksman K (2011) Characteristics of cellulose nanofibers isolated from rubberwood and empty fruit bunches of oil palm using chemo-mechanical process. Cellulose 18(4):1085–1095. https://doi.org/10.1007/s10570-011-9546-7

48. Chen S, Song Y, Xu F (2018) Highly transparent and hazy cellulose nanopaper simultaneously with a self-cleaning superhydrophobic surface. ACS Sustainable Chem and Eng 6:5173–5181. https://doi.org/10.1021/acssuschemeng.7b04814

49. Dufresne A (2013) Nanocellulose: a new ageless bionanomaterial. Mater Today 16(6):220–227. https://doi.org/10.1016/j.mattod.2013.06.004

50. Xue J, Song F, Yin X, Wang X, Wang Y (2015) Let it shine: a transparent and photoluminescent foldable nanocellulose/quantum dot paper. Appl Mater Interfaces 7(19):10076–10079. https://doi.org/10.1021/acsami.5b02011

51. Nogi M, Iwamoto S, Nakagaito AN, Yano H (2009) Optically transparent nanofiber paper. Adv Mater 21(16):1595–1598. https://doi.org/10.1002/adma.200803174

52. Hsieh MC, Koga H, Suganuma K, Nogi M (2017) Hazy transparent cellulose nanopaper. Sci Rep 7:1–7. https://doi.org/10.1038/srep41590

53. Wang Q et al (2018) Flexible cellulose nanopaper with high wet tensile strength, high toughness, and tunable ultraviolet blocking ability fabricated from tobacco stalk via a sustainable method. J Mater Chem A 6:13021–13030. https://doi.org/10.1039/C8TA01986J

54. Wang Q, Zhu JY, Considine JM (2013) Strong and optically transparent films prepared using cellulosic solid residue recovered from cellulose nanocrystals production waste stream. Appl Mater Interfaces 5:2527–2534. https://doi.org/10.1021/am302967m

55. Iwatake A, Nogi M, Yano H (2008) Cellulose nanofiber-reinforced polylactic acid. Compos Sci Technol 68:2103–2106. https://doi.org/10.1016/j.compscitech.2008.03.006

56. Amiralian N, Annamalai PK, Memmott P, Martin DJ (2015) Isolation of cellulose nanofibrils from Triodia pungens via different mechanical methods. Cellulose 22(4):2483–2498. https://doi.org/10.1007/s10570-015-0688-x

Publisher's Note Springer Nature remains neutral with regard to jurisdictional claims in published maps and institutional affiliations.